Multiprobe characterization of plasma flows for space propulsion

Damba, Julius; Argente, P.; Maldonado, P. E.; Cervone, A.; Domenech-Garret, J.L.; Conde, Luis

DOI
10.1088/1742-6596/958/1/012002

Publication date
2018

Document Version
Final published version

Published in
Journal of Physics: Conference Series

Multiprobe characterization of plasma flows for space propulsion

IOP Conf. Series: Journal of Physics: Conf. Series **958** (2018) 012002 doi:10.1088/1742-6596/958/1/012002

Multiprobe characterization of plasma flows for space propulsion

Julius Damba[1], P. Argente[1], P. E. Maldonado[2], A. Cervone[2], J. L. Domenech-Garret[1] and L. Conde[1]

[1] Departamento de Física Aplicada, ETSIAE, Univ. Politécnica de Madrid, 28040, Madrid, Spain

[2] Department of Space Engineering. Delft University of Technology. Kluyverweg 1, 2629HS Delft. The Netherlands

Abstract. Plasma engines for space propulsion generate plasma jets (also denominated plasma plumes) having supersonic ion groups with typical speeds in the order of tens of kilometers per second, which lies between electron and ion thermal speeds. Studies of the stationary plasma expansion process using a four-grid retarding field energy analyzer (RFEA), an emissive probe (EP) and a Langmuir probe (LP), all mounted on a three dimensionally (3D) displaced multiprobe structure are discussed. Specifically, the determination of plasma beam properties from the RFEA current–voltage (IV) characteristic curves is presented. The experimental results show the ion energy spectra to be essentially unchanged over 300 mm along the plasma-jet expansion axis of symmetry. The measured ion velocity distribution function (IVDF) results from the superposition of different ion groups and has two dominant populations: A low-energy group constituted of ions from the background plasma is produced by the interaction of the plasma jet with the walls of the vacuum chamber. The fast-ion population is composed of ions from the plasma beam moving at supersonic speeds with respect to the low-energy ions. The decreasing spatial profiles of the plasma-jet current density are compared with those of the low-energy ion group, which are not uniform along the axis of symmetry because of the small contributions from other ion populations with intermediate speeds.

E-mail: julius.damba@upm.es

1. Introduction

Electric propulsion (EP) has nowadays proved to be a growing technology for spacecraft propulsion. Rocket engines operate according to the basic principle of action and reaction, where the gas or plasma jet exhaust speed v_{ex} is crucial for momentum transfer. In conventional chemical thrusters, the maximum achievable gas speed is limited to the energy stored per unit mass of the propellant. EP systems overcome this limitation by use of supersonic plasma flows (also denominated *plasma plumes*) where ions accelerated by electromagnetic fields reach one to two orders-of-magnitude higher exhaust speeds. A higher specific impulse $I_{sp} = v_{ex}/g_o$, where g_o is the standard Earth acceleration, allows for a longer mission time and a heavier payload because of the reduced amount of required propellant [1, 2, 3, 4].

EP systems are characterized by large specific impulse and low thrust ($T = \dot{m}_i\, v_{ex}$) levels that rely on the mass ion production rate $\dot{m}_i$ achieved with the reduced electric power available on board. These features are essential for orbital maneuvres, station keeping, flight formation and/or end-of-life disposal of Earth-orbiting satellites. Today, hundreds of different thrusters

are being successfully used for orbit correction as well as in deep-space scientific missions. Large telecommunication satellites are nowadays the main target consumers of high-power ion engines with typical thrust levels in hundreds of milli newtons and electric power consumption within the kilowatt range [1, 2].

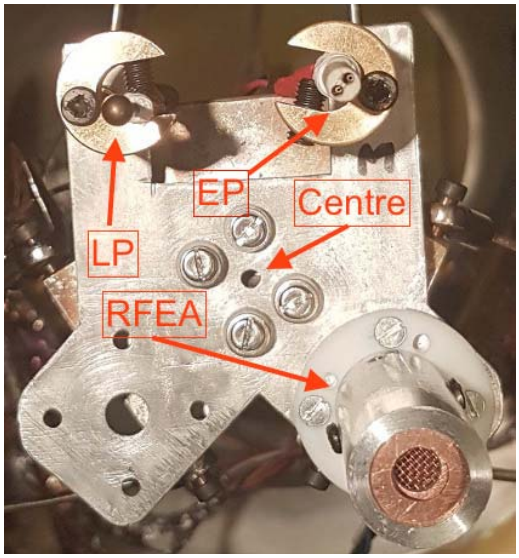

Figure 1. Front view of the multiprobe platform. The geometrical centre is indicated by the arrow.

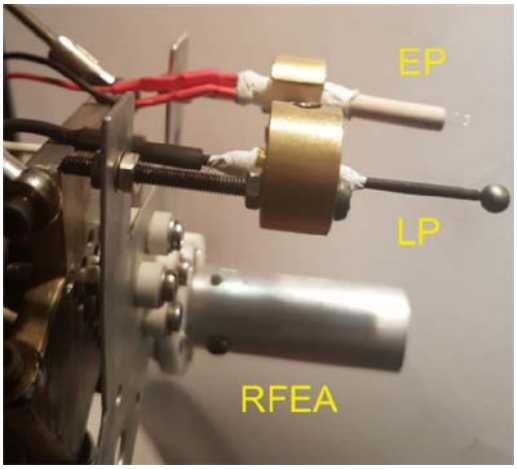

Figure 2. Side view of the LP, EP and RFEA probes mounted onto the platform, with their front ends aligned and facing the plasma thruster.

However, significant scientific and system engineering challenges are encountered during the design and integration of electric propulsion into small satellites (50–250 kg), such as the ones planned for constellations intended for global internet coverage and interactive television. These require thrust levels of roughly of 0.1–10 mN and electric power consumption below 500 W. Our alternative low power hybrid ion engine (ALPHIE) that has been the subject of a recent patent application falls within this category [5].

The outstanding characteristic of plasma thrusters for space propulsion is the acceleration of ions to supersonic speeds. This feature is investigated using the ion velocity distribution function (IVDF) of plasma streams in connection with the operational modes of the plasma thruster. The ALPHIE engine has been found to produce a mesothermal plasma flow [6] in which the exhaust plasma jet emerges with drift speeds that are intermediate between the ion and electron thermal speeds [7, 8, 9]. Such plasmas have been of great interest in recent studies of plasma flows, and are of crucial importance in electric propulsion and spacecraft–plasma interaction studies [10, 11, 12].

Also important but nevertheless not well understood characteristics are the spatial structure and physical mechanisms involved in the expansion of the plasma stream, as well as the interplays among different collisional processes (electron–neutral, ion–neutral, etc) and the ion energy relaxation mechanisms in the plasma stream. Understanding these would require pointwise measurements using a combination of different diagnostics, such as an emissive probe (EP), a Langmuir probe (LP) and a retarding field energy analyzer (RFEA) in order to obtain the spatial profiles of plasma properties like the electron density n_e, ion density n_i, plasma potential V_{sp} and the distribution of ion speeds.

In this paper we discuss the experimental results of the one-dimensional IVDF spatial profiles of mesothermal plasma flows from the ALPHIE thruster and the technical characteristics of the

computer-controlled multiprobe platform in Figs. (1) and (2). The structure of this paper is as follows: the features of the sliding positioning system are described in Sec. 2 and the electric probe diagnostics are discussed in Sec. 3. The experimental results are discussed in Sec. 4, specifically the two-peaked ion velocity spectra along the axis of symmetry of the plasma flow. Finally, we end in Sec. 5 with some concluding remarks.

2. The 3-D positioning/multiprobe system

The support structure for the positioning system fits exactly into our cylindrical stainless steel vacuum vessel of 80 cm length and 40 cm diameter, and it has the same cylindrical symmetry as the vacuum tank. The multiprobe platform that supports the measurement probes, shown in Figs. (1) and (2), is driven by three independent stepper motors.

The electric motors of the computer-controlled platform are shielded from any electromagnetic effects due to the plasma by carefully wrapping them in aluminium foils that are electrically connected to the grounded walls of the vacuum tank. Each stepper motor drives a rubber timing belt arranged inside an aluminium rail (also electrically grounded) that protects the belt from thermal loads and damage due to plasma exposure. This enables the setup to withstand long operation periods. The geometrical centre of the platform is indicated by an arrow in Fig. (1) and the combined effect of the three stepper motors produce 3-D rectangular displacements of this point with a spatial resolution better than ± 1 mm along the three spatial coordinates.

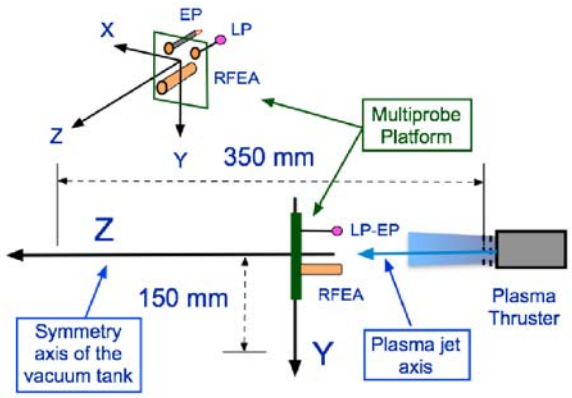

Figure 3. Schematic of the mechanical system for the multiprobe platform in Figs. (1) and (2). The probes face the plasma beam that is approximately centred at the Z-axis of symmetry.

The scheme in Fig. (3) shows the 3-D coordinate frame for the mechanical system, where the central point of Fig. (1) indicates the location of the Z axis, parallel to the symmetry axis of the vacuum tank. The mechanical system can displace the platform by 150 mm along both the X and Y directions and 300 mm along the Z coordinate axis.

As shown in Figs. (1) and (2), the probes were carefully and precisely mounted facing the plasma flow and aligned with a transversal plane to the platform. The RFEA is supported by screws whereas the LP and EP are mounted on D-shaped supports which can be released for maintenance and cleaning. However, a calibration is performed for the actual axial distances to account for the relative position of the exit section of the plasma thruster to the actual measuring range considered in Figs. (6), (7) and (8), i.e., 50– 350 mm. This ensures that the coordinates of each of the probes during measurements correspond to the real coordinates registered by the control software.

3. Plasma diagnostics

The plasma jet properties were characterized using a collecting Langmuir probe (LP) and a four-grid retarding-field energy analyzer (RFEA). The spherical stainless steel LP has a diameter of

4.44 mm and was biased with respect to the grounded walls of the vacuum tank using a time-sweep circuit.

The spherical probe was preferred to planar or cylindrical configurations to have minimum effect on the plasma jet expansion process. The probe was disposed as shown in Figs. (1–3), facing the plasma jet and its supporting shaft is oriented at the back side to minimize plasma wake effects on collected particles. Additionally, the deviation from spherical symmetry introduced by the electrically insulated support shaft of 1.33 mm diameter can be estimated using its cross sectional area. This correction is only 9% compared with the surface area of the Langmuir probe.

The LP probe was polarized by a 200 Hz frequency ramp signal added to a DC time-independent voltage [13]. The voltage–current (IV) characteristic curves were digitized by means of a Yokogawa DL9140 digital oscilloscope and stored for further analysis [13, 14, 15].

With the assumption of a Maxwellian energy distribution of electrons at 350 mm away from the plasma thruster, the typical electron densities in our experiments are in the range $n_e \simeq 0.1$–8.0×10^8 cm^{-3} with electron temperatures of $T_e = 1$–2 eV. These values give electron Debye lengths λ_{De} between 0.2 and 3.3 mm for the background plasma.

The RFEA [16, 17] operates under stationary conditions and has a 19.7 mm external diameter, with four grids that are equally spaced at $d = 5.0$ mm placed transversal to a cylindrical open channel. Ion motion in the analyzer is through this channel, which is 25.0 mm long with a cross section of 7.17 mm diameter. The ion current is collected by a copper plate located at the back end of the ion channel. The transparency of the system, T_r= 18.6%, was determined by optical methods.

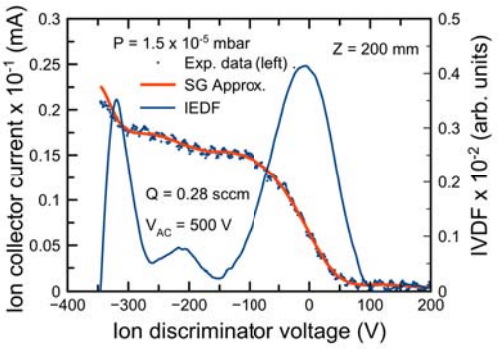

Figure 4. The original experimental data, a Savitzky-Golay numerical approximation of the IV curve (left axis) and the calculated IVDF (right axis) represented against V_{id} at $Z = 200$ mm.

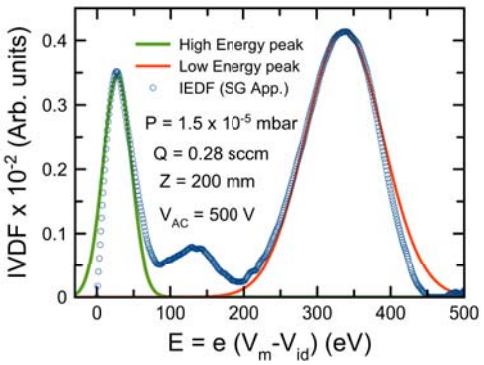

Figure 5. The IVDF (open symbols) of Fig. 4 and the two main peaks approximated by Gaussian functions (solid curves).

The RFEA voltage–current characteristic curves were obtained by measuring the ion-collector current as a function of the ion-discriminator grid voltage V_{id} relative to the (grounded) walls of the vacuum chamber. Such IV curves were digitized using a Keithley 2000 digital multimeter and a computer-controlled voltage source electrically connected to the ion discriminator grid. The typical electric potentials V_{es} and V_{er} of the secondary electron suppressor and the plasma electron repeller grids [16, 17], respectively, were $V_{es} \simeq V_{er}$= 25–30 V. These potentials repel the plasma electrons passing through the (electrically floating) RFEA first/front grid and suppress the secondary electron emission current produced by high-energy ions impacting the copper collector plate.

The ions with speeds $u_z > 0$ parallel to the axis of symmetry of the vacuum tank are collected and measured by the RFEA back plate. The ion energy resolution was about $\pm$ 8 eV for singly charged Argon ions of 400 eV energy. This is equivalent to radial speeds of ± 6 km s^{-1} for ions with axial speeds of 44 km s^{-1}.

The current density at the ion collector plate is $J_c = e\, u_z\, dn_i$, where $e > 0$ is the electronic charge; $dn_i = f(u_z)\, du_z$ is the number of ions with axial speeds between u_z and $u_z + du_z$ and $f(\boldsymbol{r}, u_z)$ is the stationary one-dimensional ion velocity distribution function at the point $\boldsymbol{r}$ where the RFEA is located. The ions reaching the collector plate have kinetic energies $E = m_i u_z^2/2 \geq eV_{id}$ to overcome the repelling potential V_{id} of the ion-discriminator grid. Hence, the ion current density collected by the RFEA copper plate is,

$$J_c(\boldsymbol{r}, u_{mz}) = e \int_{u_{mz}}^{\infty} u_z\, f(\boldsymbol{r}, u_z)\, du_z$$

Setting $dE = m_i\, u_z\, du_z$ and $s = m_i\, u_z^2/2$ we have,

$$J_c(\boldsymbol{r}, eV_{id}) = \frac{e}{m_i} \int_{eV_{id}}^{\infty} f(\boldsymbol{r}, s)\, ds \tag{1}$$

For a fixed position $\boldsymbol{r}$ the current density $J_c(\boldsymbol{r}, eV_{id})$ is a monotonically decreasing function of the discriminator voltage V_{id}. It falls from the maximum value when $V_{id} = V_m$, in which case all the ions can pass through the RFEA channel to impact the collector plate. The maximum current density $J_c(\boldsymbol{r}, eV_m)$ contains the contributions from all groups of ions in $f(\boldsymbol{r}, s)$ to the RFEA current–voltage curve. Then, $J_c(\boldsymbol{r}, eV_{id})$ in Eq. (1) decreases for $V_{id} > V_m$ because ions with low energies are rejected by the ion-discriminator grid and do not contribute to the total (integrated) current density.

The discriminator electric potential V_m that result in the maximum $J_c(\boldsymbol{r}, eV_m)$ corresponds to the lowest possible ion speed u_{mx} detected by the RFEA. The voltage V_m can be different from zero because the discriminator potentials V_{id} are not measured with respect to the local plasma potential but to the electric ground of the system. Setting $V_{id} = V_m$ in the lower limit of the integral in Eq. (1),

$$J_c(\boldsymbol{r}, eV_m) = e \int_{0}^{\infty} u_z\, f(\boldsymbol{r}, u_z)\, du_z = \frac{e}{m_i} \int_{eV_m}^{\infty} f(\boldsymbol{r}, s)\, ds \tag{2}$$

The maximum current density $J_{im}(\boldsymbol{r}) = J_c(\boldsymbol{r}, eV_m)$ can thus be calculated for each point $\boldsymbol{r}$ as,

$$J_{im}(\boldsymbol{r}) = \frac{I_m(\boldsymbol{r})}{T \times S}$$

where T_r is the transparency of the four-grid analyzer, S is the effective area of the copper collector plate and $I_m(\boldsymbol{r})$ is the maximum current of an RFEA current–voltage curve.

Furthermore, differentiating the ion current with respect to the bias potential of the ion-discriminator grid in Eq. (1) we have,

$$\frac{dJ_c}{dV_{id}} = -\frac{e^2}{m_i} f(\boldsymbol{r}, eV_{id}) \tag{3}$$

We make use of Eq. (3) in Sec. 4 to obtain the one-dimensional distribution function of the ion speeds. For this purpose, the IV curves of the RFEA were numerically approximated using the Savitzky-Golay (SG) scheme [18] to evaluate their derivatives, which are proportional to the one-dimensional IVDF in Eqs. (1) and (2).

The results of this analysis are shown in Figs. (4) and (5) where the original RFEA currents (blue dots) and their SG numerical approximation (solid curve) are represented against the bias

potential of the ion discriminator grid. The shape of the IV curves indicates the presence of different ion groups in the one-dimensional IVDF (right axis), with maximum velocities realized for bias voltages where Eq. (3) has a maximum.

As shown in Fig. (5), the ion velocity distribution function can be represented against the scaled electric potential $e\,(V_m - V_{id}) = m_i u_z^2/2$ for $V_{id} > V_m$, so that $u_z \simeq 0$ for the maximum measured current $I_m(\boldsymbol{r})$ of the RFEA current–voltage curve. The IVDF in Fig. (5) has thus been plotted against the kinetic energy of ions, as well as in Fig. (6) where the energy axis is inverted for clarity.

The IVDF as in Fig. (5) has three peaks that can be considered to be the superposition of two or more ion populations, but with only two ion groups playing a dominant role. The SG approximations of the IV curves, as in Fig. (3), along the Z axis are represented in Fig. (6). Finally, the ion temperatures can be evaluated using the full width at half maximum (FWHM) values of the Gaussian fits to the two main peaks of the IVDF as in Fig. (5).

4. Experimental results

The limited pumping speed of our vacuum equipment determines the maximum possible Argon mass flow rate for the operation of the ALPHIE plasma thruster, and consequently its ion production rate $\dot{m}_i$. However, sufficient plasma production in Argon is achieved with neutral gas flow rates as low as $Q = 0.28$ sccm (standard cubic centimeter by minute), allowing for a low gas pressure of $p_a = 1.5 \times 10^{-5}$ mbar to be achieved inside the plasma chamber as shown in Figs. (6), (7) and (8).

The multiprobe stand was employed for the precise positioning of the probes at different points $\boldsymbol{r}$ within the mesothermal plasma flow generated by our ALPHIE plasma thruster that operates under stationary conditions. Supersonic ion streams with typical speeds in the range 37–44 km s^{-1} which are higher than the characteristic ion sound velocities c_{is} =10–11 km s^{-1} at a fixed point 20 cm from the thruster exit section have been observed in previous studies [6].

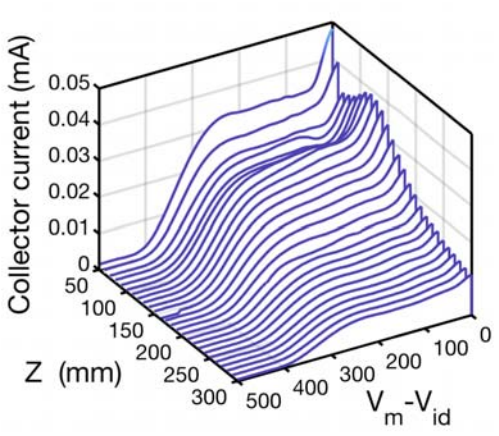

Figure 6. A waterfall representation of SG approximations of the RFEA current–voltage characteristic curves along the Z axis of the scheme in Fig.(3).

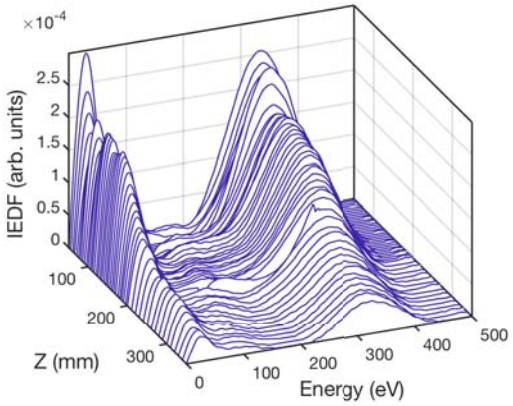

Figure 7. Waterfall representation of the two-peaked IVDFs, calculated from the IV curves of Fig. (6), along the Z axis against the kinetic energy.

These general characteristics are confirmed by the waterfall representation (see Fig. 7) of the two-peaked IVDFs of the scheme of Fig. (3) along Z which is approximately aligned with

the centreline of the plasma jet. The same distribution functions are plotted against the kinetic energy $E = e\,(V_m - V_{id})$, as shown in Fig. (5).

The maxima of the fast ion group are around 330 eV and at about 30 eV for the low-energy populations. The speeds corresponding to the low-energy ion group peaks remain essentially independent of the operational parameters of the ALPHIE thruster, whereas the velocity of the fast ions depends on the acceleration voltage [6] (which was fixed at $V_{ac} = 500$ V in this case). The velocities in Fig. (7) remain essentially constant over 50–350 mm along the axial direction. Additionally, the height of the ion velocity distribution function decreases with the radial coordinate Z as the plasma jet expands.

The characteristic cross sections for collision (elastic and resonant charge exchange) of neutral atoms with Argon ions are in the order of $\sigma_{ia} \sim 3 \times 10^{-15}$ cm^2 [19, 20], which correspond to mean free path of $\lambda_{ai} \simeq 500$ cm for our working pressures. We also obtain $\lambda_{aa} \simeq 430$ cm for elastic collisions between two neutral Argon atoms [19]. The cross sections for electron and ion impact ionization of Argon also lead to mean free paths exceeding the size of our vacuum tank [20]. Furthermore, the plasma potential variations measured with the emissive probe along the axial direction are in the order of a few volts, well below the characteristic kinetic energy of the ions in Fig. (7). Thus, there is no evidence for axial electric fields that could appreciably change the velocity of heavy particles in the plasma.

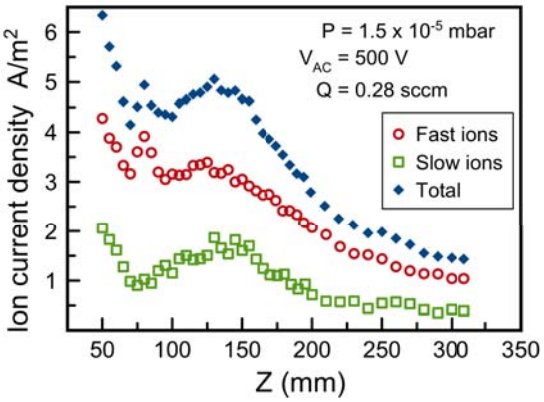

Figure 8. Current densities along the Z axis of Fig. (3), calculated from the RFEA current–voltage curves in Fig. (6). The open circles and squares show, respectively, the current densities $J_{if}(z)$ and $J_{il}(z)$ of the ions with kinetic energies above and below 200 eV. The solid diamond shapes represent the sum of the two ion group contributions.

The plasma thruster is the only source of ions in our experiment, and therefore the low-energy ion groups in Figs. (4) and (7) are due to the interaction of fast positively charged particles with the vacuum chamber walls. A number of ions from the plasma beam recombine after colliding with the walls, but a significant proportion is reflected back towards the plasma chamber after losing a large fraction of their initial energy. The resulting heavy particles, with reduced speeds, must be responsible for the formation of the low-energy peak in the IVDF. Hence, the speeds of ions in this low-energy group must be in random directions yet the ion velocity distributions in Fig. (7) only account for those with $v_z > 0$ present at the point where the RFEA is located. On the contrary, fast ions have a very important proportion of velocity components along the direction of the plasma jet expansion, parallel to the Z axis in Fig. (3).

The FWHM estimates of ion temperatures for the two main peaks in Figs. (5) and (7) give similar values along the Z axis. For the low-energy ion group we obtain $k_B T_{il} = 30$ eV, whereas $k_B T_{if} = 120$ eV for the fast-ion population. Both ion temperatures are higher than the typical electron temperatures of the distant background plasma. The kinetic energy range 200–400 eV of the fast-ion group peaks in Fig. (7) leads to ion velocities of 31–44 km s^{-1}, which are much higher than the ion sound speed $c_{is} = \sqrt{k_B(T_i + T_e)/m_i} \sim 8.5$ km s^{-1}. The average supersonic drift speed $u_D = u_{df} - u_{dl} \simeq 38$ km s^{-1} of the fast ion group can be estimated by the difference

between the average peak velocities $u_{dl} \simeq 15$ km s^{-1} and $u_{df} \simeq 53$ km s^{-1} of the slow and fast ion groups, respectively.

The axial profile of the stationary plasma jet expansion along the axis of symmetry (Z) is shown in Fig. (8), where the maximum RFEA ion current densities $J_{im}(z)$ are referred to. These values are calculated from the current maxima $I_m(z)$ in Fig. (6) and they account for the contribution to the RFEA ion current of all ion populations in the energy spectra of Fig. (7). Unfortunately, the charged-particle densities in the plasma beam cannot be estimated from the current densities in Fig. (8) because of the broad energy range in Fig. (7).

However, the current density $J_c(z, eV)$ in Eq. (2) is only due to the contribution of ions with energies $E \geq eV$ to the RFEA ion current and we make use of this fact to estimate the axial current density of ions in the plasma jet. Fig. (7) shows the two main IVDF peaks to be separated at energy $E_l \simeq 200$ eV. Therefore, $J_c(z, E_l) = j_{if}(z)$ is approximately the current density $j_{if}(z)$ of the plasma-beam ions whereas $J_{il}(z) = J_{im}(z) - J_{if}(z)$ is the contribution of low-energy ions in the IVDF to the RFEA maximum current. The values of $j_{if}(z)$ (open circles) and $J_{il}(z)$ (open squares) are also represented together with $J_{im}(z)$ (solid diamonds) in Fig. (8).

The plasma beam ion current density $J_{if}(z)$ decreases by a factor 2.7 over 300 mm along the axial direction Z that is collinear with the central direction of propagation of the plasma jet. The flow of supersonic ions is maximum close to the exit section of the plasma thruster and decreases along the axial direction. The flow due to low-energy ions $J_{il}(z)$ is spatially irregular, always less than $J_{if}(z)$ and is maximum around 150 mm. The increase in both $J_{if}(z)$ and $J_{il}(z)$ around $Z = 150$ mm results from the contribution to the measured RFEA ion current by the small peak between 100–200 eV, which can be observed in Figs. (5) and (7). The estimation of the $J_{if}(z)$ and $J_{ij}(z)$ was made by simply setting $E_l = 200$ eV which divides the contribution of this small third ion group between both current densities.

5. Conclusions

We have been able to show how a combination of the three diagnostics on the movable multiprobe platform constitutes a valuable tool to explore the plasma expansion process for supersonic plasma jets. Plasma beam diagnostics requires a combination of different probes since the RFEA which is the conventional tool for plasma energy analysis has a directional character. Only heavy charged particles with speeds parallel to RFEA axis are detected at its end collector plate. Therefore, the displacement of the RFEA axis should reflect the symmetry of the plasma expansion process. In view of this, the RFEA diagnostic needs to be complemented with emissive and Langmuir probes to obtain a complete physical picture of the plasma expansion process.

Here we focused our attention on the determination of plasma properties along the Z axis shown in the schematic of Fig. (3). This axial direction represents the symmetry of collimation of the hemispherical expansion of the plasma jet, allowing reliable measurements of the IVDF with the RFEA. The velocity distribution functions of ions in Fig. (7) confirm the general characteristics of the mesothermal plasma jets produced by the ALPHIE plasma thruster previously observed [6].

As we have shown, two ion groups dominate the expansion of ALPHIE plasma jets along the axial direction. The preserved ion velocity distribution functions in Fig. (7) along the Z axis indicate how the supersonic ion group remains essentially unchanged and is only modified by the interaction with the vacuum chamber walls. The low-energy peak in the IVDF corresponds to ions reflected back from the walls with lower energies. Unfortunately, we are not in position to explain the physical origin of the additional low peaks in Fig. (7) at intermediate energies of 100–200 eV that appear at some points. The ion energy losses by collisional energy exchange are excluded because of the long mean free paths required.

Future work will address the determination of plasma jet radial dependence of the IVDF and their influence on beam collimation, as well as the study of the electron energy distribution

functions.

Acknowledgments
The authors are indebted to Dr. J. González for his useful suggestions. The technical assistance from Mr. F. Sánchez is also appreciated. This work was funded by the Ministerio de Economía, Ciencia e Innnovación of Spain under Grant ESP2013–41078-R. The authors also acknowledge the financial support from Aernnova Aerospace SAU.

References

[1] Goebel D M and Katz I 2008 *Fundamentals of electric propulsion. Ion and Hall thrusters* (John Wiley & Sons, Hoboken, New Jersey, USA) Chaps. 1, 6 and 7
[2] Mazouffre S 2016 *Plasma Sources Sci. Technol.* **25** 033002–1,27
[3] Charles C 2009 *J. Phys. D: Applied Phys.* **42** 163001–1,18
[4] Ahedo E 2011 *Plasma Phys. Control. Fusion* **53** 124037–1,18
[5] Conde L, Domenech-Garret J L, Donoso J M, Del Río E and Castillo M A 2015 Plasma accelerator with modulated thrust. Patent application PCT/EP2015/074879. European Patent Office (2015)
[6] Conde L, Domenech-Garret J L, Donoso J, Damba J, Tierno S P, Alamillo-Gamboa E and Castillo M A 2017 Supersonic plasma beams with controlled speed generated by the alternative low power hybrid ion engine (ALPHIE) for space propulsion.
[7] Zhang Z, Tang H, Zhang Z, Wang J and Cao S 2016 *Rev. Sci. Instrum.* **87** 123510–1,8
[8] Hu Y and Wang J 2015 *IEEE Transactions on Plasma Science* **43** 2832–2838
[9] Merino M and Ahedo E 2015 *IEEE Trans. on Plasma Sci.* **43** 244–251
[10] Charles C and Boswell R W 2004 *Phys. Plasmas* **11** 1706–1714
[11] Charles C, Boswell B W and Lieberman M A 2006 *Appl. Phys. Lett.* **89** 261503–1,3
[12] Corr C S, Zanger J, Boswell B W and Charles C 2007 *Appl. Phys. Lett.* **91** 241501–1,3
[13] Troll O, Conde L, Criado E, Donoso J M and Herdrich G 2010 *Contrib. Plasma Phys.* **50** 819–823
[14] Tierno S P, Domenech-Garret J L, Donoso J M, Jennewein D, Herdrich G, Fasoulas S and Conde L 2013 *IEEE Trans. on Plasma Sci.* **41** 695–700
[15] Hershkowitz N 1989 *Plasma Diagnostics. Discharge Parameters and Chemistry.* vol 1 ed Auciello O and Flamm D L (Academic Press, San Diego, CA, USA) chap 3, pp 113–182
[16] Böhm C and Perrin J 1993 *Rev. of Sci. Instrum.* **64** 31–44
[17] Hutchinson I H 1990 *Principles of plasma diagnostics.* (Cambridge University Press, New York, USA)
[18] Magnus F and Gudmundsson J T 2008 *Rev. Sci. Instrum* **79** 073503–1,8
[19] Raizer Y P 1991 *Gas Discharge Physics* (Springer Verlag, Berlin, Germany)
[20] Lieberman M A and Lichtenberg A J 1994 *Principles of Plasma Discharges and Materials Processing.* (John Wiley & Sons,, New York, USA)